

## Non-Monoexponential Diffusion Signal Decay in Prostate Cancer

S. E. Maier<sup>1</sup>, Y. Tang<sup>1</sup>, L. P. Panych<sup>1</sup>, R. V. Mulkern<sup>2</sup>, and C. M. Tempany<sup>1</sup>

<sup>1</sup>Radiology, Brigham and Women's Hospital, Harvard Medical School, Boston, MA, United States, <sup>2</sup>Radiology, Children's Hospital, Harvard Medical School, Boston, MA

### Introduction

Non-invasive, multiparametric characterization of prostate cancer with MR imaging methods is an active area of research with great potential. Detailed studies of the diffusion of water within prostate tissues, which go beyond the basic apparent diffusion coefficient maps and incorporate information from non-monoexponential diffusion signal decays, may offer a unique ability to characterize prostate cancer. In this work we demonstrate that such studies can be performed in clinically feasible scan times and that biexponential diffusion signal decay parametrization is useful for differentiation of prostate cancer from normal peripheral zone (PZ). The methods proposed may ultimately prove of value as surrogate measures not only for the presence of cancer but also for overall tumor activity.

### Materials and Methods

**MR scanning:** Ten men with biopsy proven prostate cancer were scanned with a GE 3 Tesla MR system. Informed consent was obtained from each subject according to the local IRB committee. Diffusion imaging with whole gland coverage using an endorectal RF coil was performed with the single-shot echo-planar diffusion imaging sequence provided by the equipment manufacturer. To achieve a shorter echo time, the scan scheme for gradient directions and b-factors was modified so that diffusion encoding gradients along the three main axes were employed simultaneously with relative strength 1, 1, and 0.5. This scheme was applied along each of three orthogonal directions and for 16 evenly spaced b-factors between 0 and 3500 s/mm<sup>2</sup>. Imaging parameters were: 6 mm slice thickness, 1 mm gap, 180 x 110 mm FOV and 64 x 40 acquisition matrix, 85 ms TE. The 2.8 mm in-plane resolution was selected to ensure sufficient SNR even at the highest b-factors. With a TR of 2500 ms, the resulting total scan time was slightly under 2 minutes. T1 and T2-weighted images were obtained as part of the standard clinical protocol.

**Image processing and analysis:** Image data was transferred for off-line data fitting and image analysis. The geometric mean of the diffusion signals along three orthogonal encoding directions was computed. Subsequently, the decaying mean signal S vs. increasing b-factor was fitted with biexponential functions of the form  $S=S_0(f_f \exp(-D_f b) + f_s \exp(-D_s b))$ , where  $D_f$  and  $D_s$  denote the fast and slow diffusion coefficients and  $f_f$  and  $f_s$  ( $f_f+f_s=1$ ) the respective component size fractions of  $D_f$  and  $D_s$ . For optimal fitting results, the non-linear least-square Levenberg-Marquardt method was employed. For each subject a normal and a tumorous region-of-interest (ROI) within the PZ were identified by a radiologist using diffusion weighted images, conventional T2- and T1-weighted images as well as available biopsy reports as guides. Mean diffusion component fraction  $f_s$  and the diffusion coefficients  $D_f$  and  $D_s$  were determined for each ROI. Differences between normal and tumor tissue diffusion parameters were statistically evaluated with paired t-tests.

### Results

Interpretable data was obtained in all patients. Image parameter settings resulted in adequate SNR within the PZ for b-factors up to 3500 s/mm<sup>2</sup>. Figure 1 shows images of a patient with a tumor lesion in the PZ. The average normal ROI size was 43 mm<sup>2</sup> (20-82 mm<sup>2</sup>) and the average tumor ROI size was 40 mm<sup>2</sup> (11-131 mm<sup>2</sup>). In the presumed normal tissue, diffusion parameters  $D_f=2.32\pm 0.23 \mu\text{m}^2/\text{ms}$ ,  $D_s=0.36\pm 0.08 \mu\text{m}^2/\text{ms}$  and  $f_s=0.17\pm 0.04$  were observed. In the tumor ROIs,  $D_f$  and  $D_s$  were not significantly different from the values measured in the normal appearing PZ ROIs, i.e.,  $D_f=2.22\pm 0.72 \mu\text{m}^2/\text{ms}$ ,  $D_s=0.36\pm 0.16 \mu\text{m}^2/\text{ms}$ , whereas the slow diffusion component size fraction  $f_s=0.43\pm 0.09$  was significantly higher ( $p<0.0001$ ).

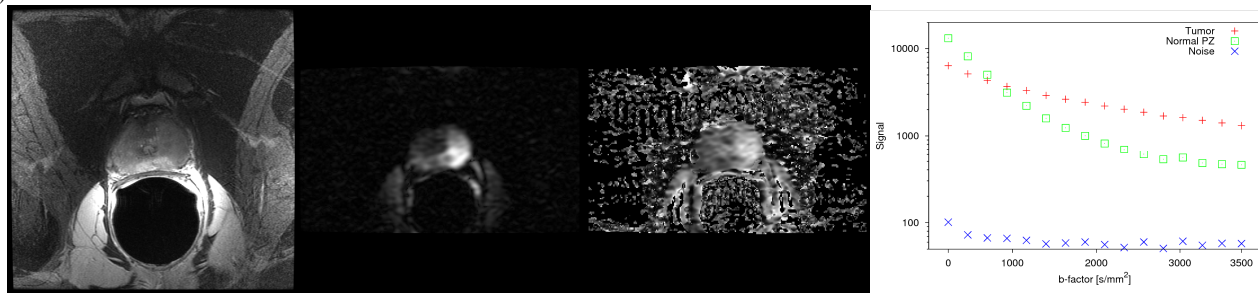


**Figure 1:** (from left to right) T2-weighted FSE image, Trace DWI 3500 s/mm<sup>2</sup>, slow diffusion component fraction  $f_s$ , and graph with typical diffusion signal decay curves for tumor, normal PZ, and noise floor values measured within ROIs.

### Discussion

Our findings are consistent with earlier observations of a non-monoexponential diffusion signal decay in prostate tissue [1] and prostate tumor tissue as measured with a single column sampling technique [2]. Our major finding is that cancerous regions do not have distinctly different fast or slow diffusion coefficients, but rather exhibit a larger proportion of slowly diffusing water molecules. The conventional dogma that the apparent diffusion coefficient decreases in prostate cancer is thus based on an incomplete interpretation. We interpret our primary result as indicative of an increase of restricted or hindered diffusion as a consequence of the presence of cancer cells. The normal milieu of the glandular PZ is as expected from histology, associated with a high fraction of freely diffusing water molecules, which when disrupted by the presence of cancer cells reveals itself as a dramatic increase of the slow diffusion component fraction. Tumor activity and cell size may be correlated with the biexponential diffusion parameters. The degree to which the relatively large variation of  $f_s$  we observed is related to such cancer properties versus simple partial volume effects remains to be assessed. This work, nevertheless, demonstrates that such an assessment is now possible in the clinical setting.

**References:** [1] Mulkern et al., Magn Reson Imag 24 (2006), 563-568. [2] Shinmoto et al., Magn Reson Imag 27 (2009) 355-359.

**Acknowledgement:** Support by NIH grants R01-EB006867 (SEM), R01-EB010195 (SEM), P41-RR019703, P01-CA067165, and R01-CA111288 (CMT)